JET–P(99)39

H Y Guo et al

Effects of Divertor Geometry and Chemical Sputtering on Impurity Behaviour and Plasma Performance in JET

JET–P(99)39

Effects of Divertor Geometry and Chemical Sputtering on Impurity Behaviour and Plasma Performance in JET

H Y Guo[1], G F Matthews, I Coffey, S K Erents, M Groth[2], P J Harbour, M von Hellermann, L D Horton, L C Ingesson, K D Lawson, J Lingertat, C F Maggi, G M McCracken, R D Monk, P D Morgan, M F Stamp, P C Stangeby[3], A Taroni, G C Vlases[1].

JET Joint Undertaking, Abingdon, Oxfordshire, OX14 3EA, UK.
[1]Redmond Plasma Physics Lab., University of Washington, Redmond, USA.
[2]and University of Manchester (UMIST), Manchester, M60 1QD, UK.
[3]and University of Toronto, Institute of Aerospace Studies, Toronto, Canada.

Preprint of a Paper to be submitted for publication in Nuclear Fusion

November 1999

ABSTRACT

The effects of increased geometrical closure on the behaviour of the recycling and intrinsic impurities are investigated in JET MkI, MkIIA and MkIIGB pumped divertors. Increasing the divertor closure leads to a significant improvement in exhaust for both deuterium and recycling impurities. However, the impurity enrichment in the exhaust gases remains unchanged due to simultaneous increase in deuterium and impurity compression in the divertor. The comparison is made for He, Ne and Ar under different plasma conditions. In addition, the operation of the Mark II and Mark IIGB divertors has shown that Z_{eff} is reduced with the improved divertor closure in the L-mode discharges, although no obvious changes in the Z_{eff} values have been observed in the ELMy H-modes. The divertor target surface temperature has a strong influence on the intrinsic carbon production. The carbon source in the Mark II and Mark IIGB divertors is significantly higher than that in the Mark I divertor, which is attributed to the enhanced chemical sputtering at the increased divertor tile temperature of the Mark II and Mark IIGB divertors (related to the divertor cooling system), as opposed to the increased closure. The consequences of this elevated yield for plasmas under different operation conditions are discussed, and further evidence, obtained from a specific wall/divertor temperature reduction experiment, is presented. The effect of the divertor screening for the chemically produced impurities is investigated using the EDGE2D/NIMBUS/DIVIMP codes for the different recycling regimes and the comparisons are made with the experimental observations from Mark I and Mark II taking into account the change in the chemical sputtering yield due to the different tile temperatures of the Mark I and Mark II divertors.

1. INTRODUCTION

The principal objectives for operating pumped divertors are to provide sufficient particle exhaust for density control and to simultaneously maintain efficient screening for the impurities produced at the divertor target plates. In addition, pumping is essential for helium ash removal from a fusion reactor such as ITER [1,2]. Adequate exhaust of He ash for ITER requires the following criteria to be satisfied [2]:

- $\tau^*_\alpha / \tau_E \leq 10$, where τ^*_α is the global alpha particle confinement time and τ_E is the energy confinement time;
- $\eta_{He} = \left(p_{He}/2p_{D2}\right)_{div} \Big/ \left(n_{He}/n_e\right)_{cor} \geq 0.2$, where η_{He} is the helium enrichment factor, the ratio of the helium concentration in the divertor to the helium concentration in the core. This condition is required in order to reduce plasma dilution, to minimise the required pumping speed, and to reduce tritium recirculation.

The impurity content of a plasma is determined by the impurity source distribution, as well as various transport processes of impurities in the SOL and the core plasma. For most materials, the dominant impurity production process is physical sputtering whilst for graphite,

chemical sputtering has also proven to be important [3,4]. This has important implications for the divertor lifetime and tritium retention [5]. Both physical and chemical sputtering depend on the energy and the mass of the impinging species. In addition, chemical sputtering depends on surface temperature [6] and exhibits an uncertain flux dependence [7-12]. The divertor screening for the impurities relies on the large ion flow present in the divertor resulting from local flux amplification due to recycled neutrals, which drags impurities toward the divertor targets, and opposes the thermal gradient force which tends to drive the impurity ions towards the main chamber [13,14]. Thus the divertor screening is sensitive to the background plasma conditions. In the normal high recycling regimes, the shielding for the divertor impurity source is strong and the wall source makes a significant contribution to the core contamination [15], in contrast to the low recycling regime where the impurity leakage from the divertor is important [16].

It is expected that increasing the divertor geometric closure to the escape of recycling neutrals should reduce the main chamber neutral fluxes, which in turn is expected to result in a reduced wall impurity source as a result of reduced neutral particle sputtering in the main chamber. At the same time, increasing the divertor closure is expected to lead to increased neutral pressure in the divertor, thus facilitating pumping. However, improved closure may also lead to reduced parallel flow in the SOL due to reduced neutral recycling to the main chamber, resulting in poor removal of impurities from the main chamber. Also, in steady state operation the improved exhaust rate must be balanced by additional particle input, usually introduced by external gas puffs, which could produce an excessive neutral source near the edge of the plasma, thus partly offsetting the effect of the closure. Furthermore, there may be problems from the interactions of ELMs with the components forming the narrow entrance of a closed divertor. In addition, there may be a source of impurities from the tokamak walls due to ion flux in the outer SOL which does not enter the divertor.

JET has investigated three pumped divertor configurations that have progressively increased geometry closure to the escape of recycling neutrals from the divertors [17,18]: Mark I (1994-95), Mark IIA (1996-97) and Mark IIAP, which is an upgraded version of Mark IIA divertor with plugged leakage paths for neutrals between the sub-divertor and the main chamber, Mark IIGB (1998-99). The

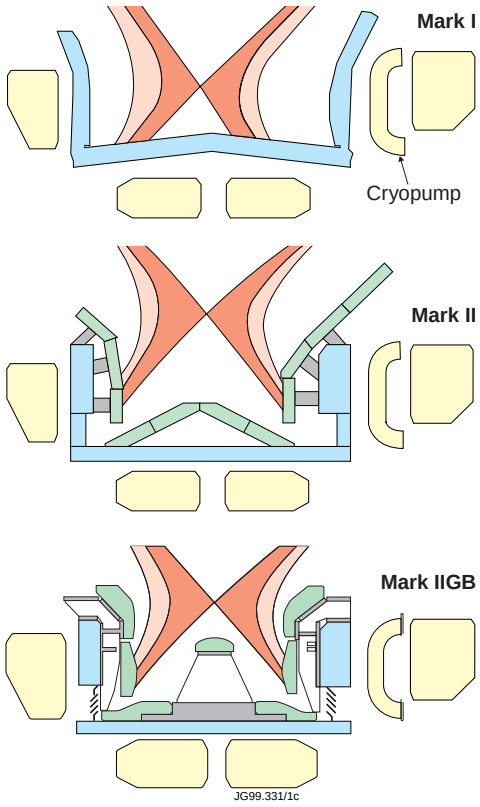

Fig.1: Poloidal cross sections of the JET Mark I, Mark II and Mark IIGB pumped divertors.

poloidal cross-sections of the Mark I, Mark II and Mark IIGB divertors are shown in Fig. 1. Where no distinction is made between Mark IIA and Mark IIAP, Mark II refers to both divertors in the present paper. As expected, one of the most noticeable consequences of increasing the divertor closure is to increase the divertor neutral pressure [19, 20]. Details of these measurements, and in particular, the effects of increased divertor closure on the impurity exhaust will be discussed.

In going from the Mark I divertor to the Mark II divertor, one unexpected result is that the impurity production yield was increased by about a factor of two, as compared with Mark I. One possible explanation for this elevated sputtering yield is the enhanced chemical sputtering in Mark II due to the higher base temperature of the Mark II target plate. Water cooled rails kept the base temperature (before plasma shots) of the Mark I tiles to ~ 40 °C whereas in Mark II thermal isolation from the cooled substructure leads to a base temperature of ~ 220 °C. Specific experiments with reduced wall and divertor temperatures were carried out with the Mark II divertor to address this issue.

The outline of the present paper is as follows. In Section 2 we report the effects of increased geometrical closure on the impurity exhaust and enrichment for the recycling impurities: He, Ne and Ar. The effect of the divertor closure on the intrinsic carbon impurity behaviour is also assessed. In Section 3 we attempt to explain the difference in the impurity production between the Mark I, Mark II and Mark IIGB divertors in terms of chemical sputtering and show further evidence coming from the wall/divertor temperature reduction experiments. The consequences of the elevated impurity yield for the plasmas under different operating conditions are discussed, hence demonstrating the significance of the impurity production for the plasma performance. In addition, the divertor screening efficiency for the impurities produced by physical and chemical sputtering processes is assessed for the different recycling regimes through detailed modelling using the EDGE2D/NIMBUS/DIVIMP codes. The summary and conclusions follow in Section 4.

2. EFFECT OF DIVERTOR GEOMETRY

2.1. Particle throughput

Increasing the divertor closure in JET has led to a significant increase in the neutral pressure in the subdivertor (the volume below the divertor target), thus improving deuterium pumping. Consequently, more gas has to be injected to maintain similar plasma densities with increased divertor closure. To illustrate this, Fig. 2 shows the neutral pressure in the subdivertor volume, as well as the gas puff rate, as a function of the plasma line averaged density for L-mode discharges in the Mark II and Mark IIGB divertors with different magnetic configurations. As expected, the divertor closure to the escape of neutrals is most effective in the regime of high plasma densities, i.e., in the high recycling not-detached regime where the electron temperature is relatively low and the density is high in the divertor so that mean-free paths of neutrals before

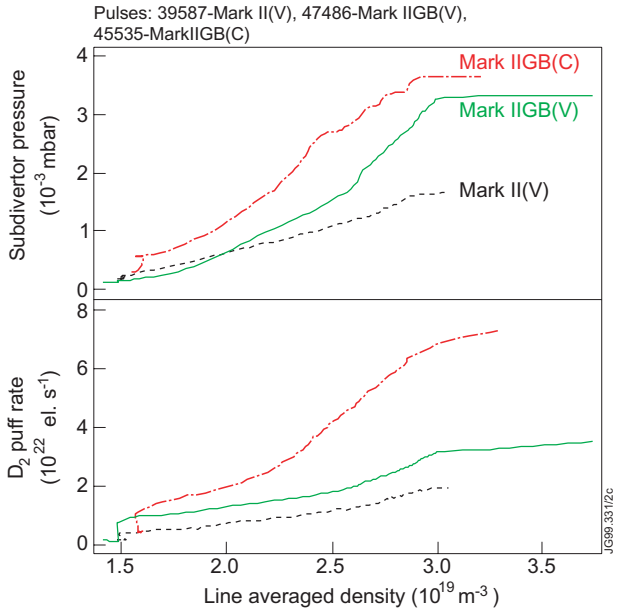

Fig.2: Subdivertor neutral pressures and gas injection rate for comparable L-mode discharges in the Mark II and Mark IIGB divertors.

ionisation are small compared to the divertor geometric size. As can be seen, for the same vertical target configuration, indicated by (V) in the figure, the divertor pressure in the Mark IIGB divertor is improved by nearly a factor of two at high densities. The pressure in the subdivertor volume is also dependent on the gas puff location [21] and the geometry of the strike points relative to the pumping ducts. A further improvement in the divertor exhaust rate was achieved in Mark IIGB with the corner configuration, (C) in the figure, where the strike points were placed next to the entrance of the pumping ducts. The difference in subdivertor pressure is less evident in the steady state ELMy H-mode discharges due to the presence of ELMs [19].

2.2. Impurity exhaust

In order to investigate impurity exhaust, we have carried out a series of dedicated experiments in L-mode plasmas using neon as a trace impurity. In these experiments, a small quantity of neon was puffed into the SOL to ensure that the perturbation of the background plasma was small. Fig. 3 shows the evolution of Ne VII line intensity following a short Ne puff into the SOL, together with the subdivertor pressure and plasma density for the discharges carried out in Mark I, Mark II and Mark IIGB divertors, respectively. The discharges have similar neutral beam heating power (~2MW) and plasma density. It can be seen that the neon exhaust rate is improved with the increased divertor closure from Mark I → Mark II → Mark IIGB, and correlates with the progressive increase in the subdivertor pressures (and thus with the divertor pumping).

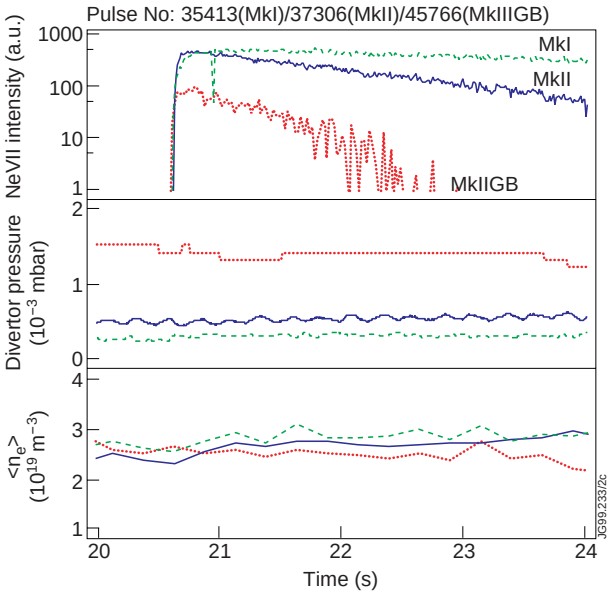

Fig.3: Time traces of L-mode discharges in Mark I, Mark II and Mark IIGB divertors, illustrating the changes in neon decay time following a short trace-neon puff.

For a given divertor geometry, the impurity exhaust is strongly dependent on the background plasma conditions. Fig. 4 shows the time traces of two identical L-mode discharges but with D_2 fuelling from different

locations:the divertor and the top of the machine, respectively. Neon was introduced from the same position (midplane) in the main chamber using gas puffs for both discharges. In each discharge, the neon was injected during the two steady-state phases with different plasma densities. We see that the decay of neon content in the plasma is strongly dependent on the plasma density or the divertor pressure, but not very sensitive to the gas puff locations. It should be noted that the ion fluxes to the divertor target are nearly identical for the two discharges, as indicated by the ion saturation current measured by the Langmuir probe near the outer strike point. However, the subdivertor pressure is higher in the divertor fuelling case, which it seems unlikely can be attributed to the recycling neutrals. Therefore, the direct bypass flow of the puffed gas to the subdivertor must contribute to the observed difference. In fact, more gas had to be puffed into the divertor to maintain the same plasma density, compared to the top fuelling case.

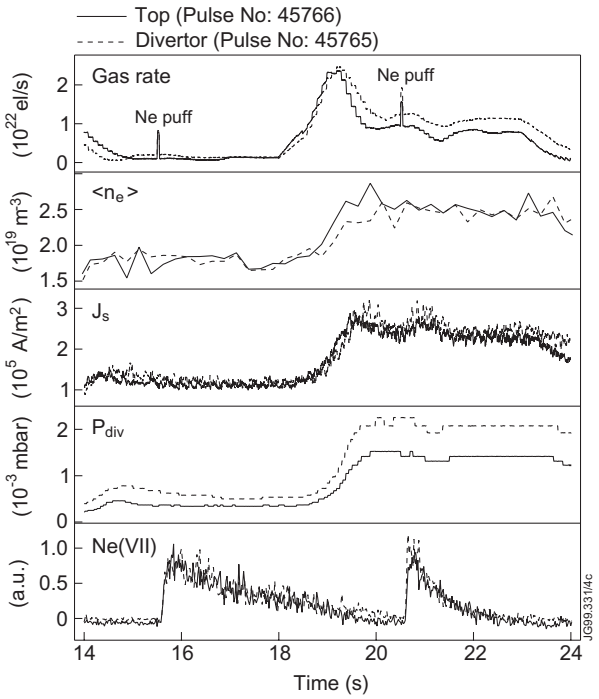

Fig.4: Time traces of two identical L-mode discharges with 2MW of neutral beam heating, but with D_2 fuelling from different locations. The data shown are the gas injection rate, the plasma volume averaged density, the ion saturation current measured by the target Langmuir probe located near the outer strike point, the subdivertor neutral pressure and Ne VII (465.22Å) intensity.

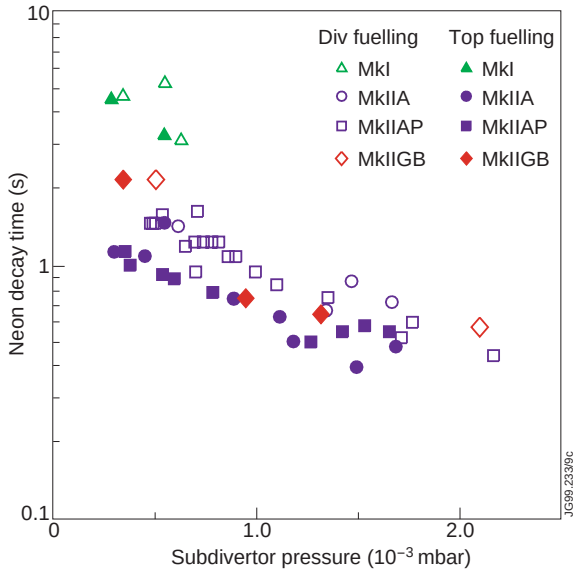

Fig.5: Neon decay time versus subdivertor pressure for the different divertor configurations, with D_2 fuelling from top and divertor respectively.

Fig. 5 shows the e-folding decay time of neon versus the subdivertor pressure for the L-mode discharges with different divertor configurations. Neon exhaust rates show a clear dependence on the subdivertor pressure and the data from the different divertors produce the same trend. Since the impurity removal rate depends on the partial pressure of the impurities in the subdivertor (next to the divertor cryopump), this would suggest that neon impurity enrichment

(ratio of the impurity concentration in the subdivertor to the core impurity concentration) is relatively insensitive to the changes in divertor configuration, as will be discussed in the next section. The recent studies for the reduced-cost ITER show that the helium concentration upstream is mostly dependent on the DT throughput and a minimum throughput of 200 Pa m^3/s is required to satisfy the constraint on the helium concentration (6%) [22]. Hence, increasing divertor closure would reduce the requirement for pumping speed for a given throughput (due to increased divertor neutral pressure).

It was expected that injecting deuterium from the top of the machine coupled to the divertor pumping should induce an ion (deuterium) flow in the SOL to enhance the frictional drag on the impurities, thus increasing impurity retention in the divertor, i.e., so called "puff and pump" concept. However, it appears that there is only a small difference in neon decay time between the top and divertor fuelling cases in the Mark II and Mark IIGB divertors (Fig. 5). One possible explanation for this is that the large intrinsic flows, which are present in the SOL, would dominate the flow achievable by D_2 fuelling. Measurements from the reciprocating probe located at the top of the machine show a significant plasma flow with Mach number of 0.35 to 0.6 in the JET SOL for a variety of plasma conditions [23].

In contrast, an increase in neon exhaust by a factor of 3 has been observed in DIII-D using top fuelling and simultaneous pumping [24,25], which was attributed to an externally induced SOL flow, and this puff and pump technique has been found most effective for high Z impurities, such as argon [26]. In ASDEX-Upgrade, no or a much smaller effect was observed using the puff and pump technique [27,28], similar to JET. These results are presently not fully understood and need further investigation.

2.3 Impurity enrichment

The impurity enrichment, i.e., $\eta_{He} = \left(p_{He}/2p_{D2}\right)_{div} \Big/ \left(n_{He}/n_e\right)_{cor}$, is derived from the ratio of the partial pressure in the subdivertor volume, measured by Penning gauge spectroscopy [29], to the core plasma concentration, determined by Charge Exchange Recombination Spectroscopy (CXRS) [30]. Helium enrichment studies have been performed under both L- and ELMy H-mode conditions in the Mark II and Mark IIGB divertors. For the L-mode discharges the helium enrichment decreases with the subdivertor pressure and also depends upon the strike point position. Preferential enrichment is obtained as the strike point is moved towards the pumping entrance slot [29]. In the case of ELMy H-modes, the enrichment is less sensitive to the strike point position. In going from Mark II to Mark IIGB, helium compression is increased, but the enrichment changes little due to the simultaneous increase in subdivertor neutral pressure. As an example, Fig. 6 shows two L-mode vertical target discharges in the Mark II and Mark IIGB divertors with the same neutral beam heating power (2MW), similar plasma density, to illustrate the changes in the subdivertor pressure (P_{div}), helium compression, i.e., $n_{He}^{div}/n_{He}^{cor}$,

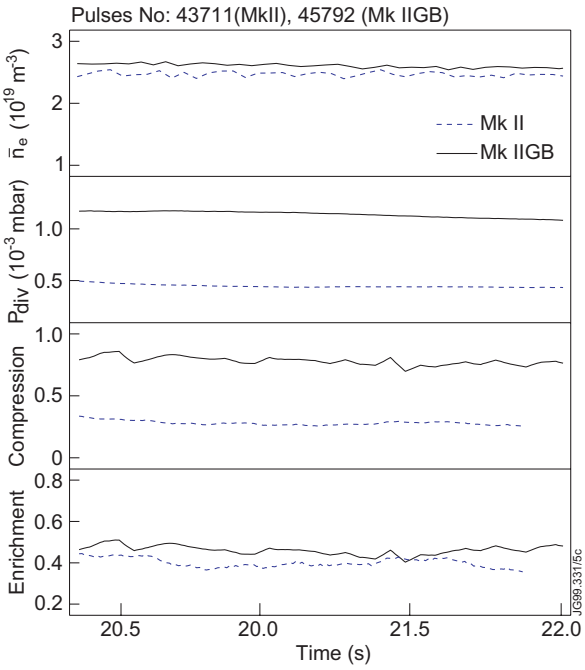

Fig.6: He enrichment, He compression ($n_{He}^{div}/n_{He}^{cor}$) and subdivertor pressures in two comparable L-mode discharges in Mark II and Mark IIGB.

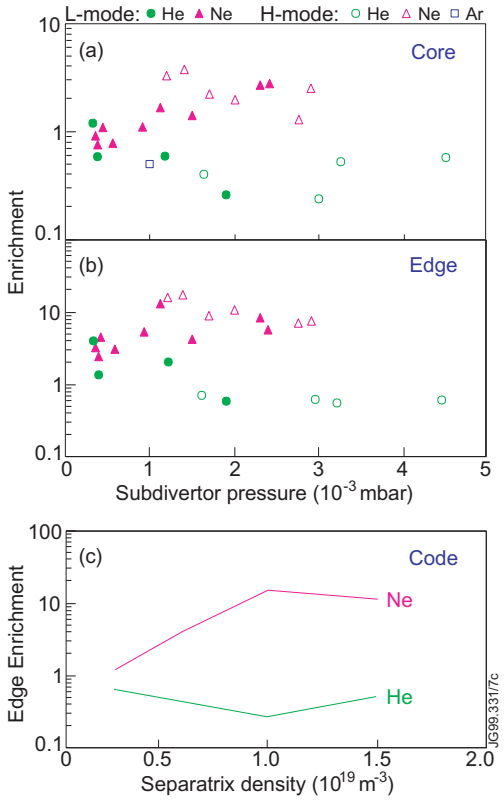

Fig.7: Measured core (a) and edge (b) enrichment factors for He/Ne/Ar in MkII GB, together with the EDGE2D results (c).

and helium enrichment. n_{He}^{div} is the helium density in the subdivertor derived from the Penning gauge measurements assuming room temperature conditions; n_{He}^{cor} is the helium density in the core plasma measured by CXRS at $\rho \approx 0.3$.

Detailed comparisons have been made for the enrichment factors between helium and other recycling impurities, i.e., neon and argon in the Mark IIGB divertor. Fig. 7 shows the enrichment factors based on densities in the core plasma, as well as the values measured at the edge of the confined plasma, at $\rho \approx 0.9$ for He/Ne/Ar impurities as a function of the subdivertor pressure in both L- and H-modes discharges. It appears that helium, neon and argon have similar enrichment factors at low subdivertor pressure, or plasma density. The enrichment for neon in L-mode discharges is observed to increase as the subdivertor pressure is increased, in contrast to the helium enrichment, so that higher enrichment factors are achieved for neon than for helium at high subdivertor pressure. In the H-mode discharges, the enrichment factors for both neon and helium exhibit no clear trends. However, increased enrichment for neon can be clearly seen, despite a large scatter. Whilst the enrichment for neon is generally above unity, except at very low subdivertor pressures, a significant de-enrichment (η_{He} <1) is observed for helium. The reason for this difference [31] is that the He neutrals have a longer mean-free path before ionisation compared to deuterium or neon. Thus the He-ions tend to be created above the point where the plasma flow toward the divertor target is strong, and the frictional drag toward the plate is

therefore weaker. The ion gradient force, directed upstream, tends to be more important, causing more divertor leakage for helium than for other impurities. Nevertheless, in all the cases studied, helium enrichment is above the minimum requirement for ITER, i.e., $\eta_{He} \geq 0.2$.

We have employed the 2-D fluid EDGE2D/NIMBUS codes [32] to simulate the enrichment for helium and neon in typical L-mode plasmas with the following input parameters: P_{sol} = 2MW, n_{sep} = 0.3-1.5×10^{19} m^{-3}, $D_{\perp}$ = 0.2 m^2/s and $\chi_{\perp}^{i,e}$=0.5 m^2/s (in flux space). The intrinsic carbon content is controlled by both physical and chemical sputtering. The chemical sputtering yield is taken from the work of the University of Toronto group [6] with a yield reduction factor of 0.5 (in order to allow for some effect of molecular hydrocarbon fragments suppression at high incidence flux, and for prompt redeposition). Thus the effective sputtering yield is given by: $Y_{eff} = Y_{phys} + 0.5\ Y_{chem}^{Toronto}$. More details on the impurity source modelling will be described in Section 3.5. As in the experiments, only small quantities of helium and neon are introduced into the SOL so that the background plasma parameters are little changed due to the presence of neon. The calculated enrichment factors, relative to the edge impurity concentration, are shown in Fig. 7 (c) as a function of the separatrix density. The code reproduces the observed trends and also the absolute values for both helium and neon. In particular, the calculated results show that neon enrichment increases with separatrix density and rolls over at sufficiently high densities, in contrast to helium enrichment, consistent with experimental observations.

2.4. Intrinsic impurity behaviour

The increased divertor closure improves the plasma purity in the L-mode discharges, as expected. Fig. 8 compares the Z_{eff} and the radiated power (P_{rad}) between Mark II and Mark IIGB divertors for L-mode discharges with the same vertical target configuration and the same additional NB heating (~2MW). The Z_{eff} values are derived from the bremsstrahlung emission at 523 nm and the radiated power is obtained from the tomography reconstruction. As can be seen, Z_{eff} is reduced from Mark II to Mark IIGB. As a result, the radiation is reduced at a given plasma density. Note that the Z_{eff} measurements are subject to large uncertainties (up to 30%). However, the data from the CXRS show similar trends. In addition, the L-mode density limit is improved in the Mark IIGB discharge

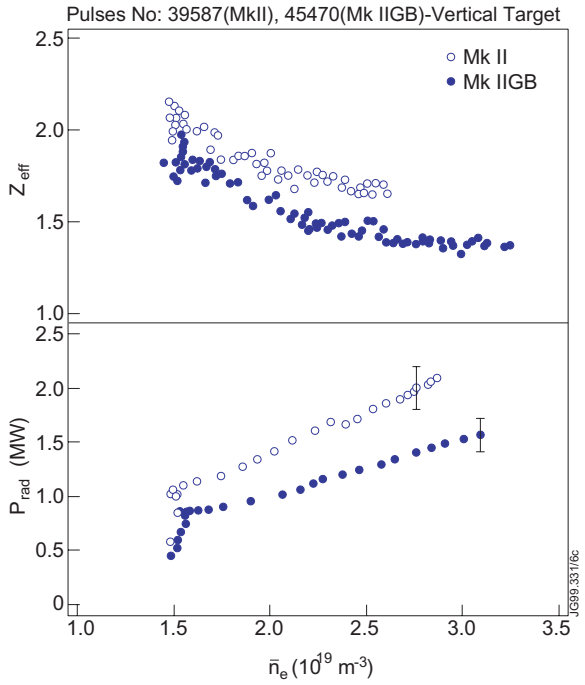

Fig.8: Z_{eff} and P_{rad} against plasma line averaged density for L-mode discharges in the Mark II and Mark IIGB divertors.

compared to the Mark II case (as will be discussed in Section 3.2). This further confirms the improved plasma purity in the Mark IIGB divertor.

No obvious changes in Z_{eff} have been observed in the ELMy H-modes [20, 33]. Some possible explanations for this are as follows: as the divertor becomes geometrically more closed, ion impact during an ELM can lead to stronger impurity sputtering at the components forming the narrow entrance of the divertor where impurities can more efficiently contaminate the core, compared to the impurities originating at the target plate. In addition, the impurity sources in the Mark II divertor is higher than that in the Mark I divertor, hence offsetting the effect of the divertor closure, as will be discussed in the following section.

3. EFFECT OF DIVERTOR SURFACE TEMPERATURE ON IMPURITY PRODUCTION AND PLASMA PERFORMANCE

3.1 Divertor carbon source

Divertor operation leads to strong interaction of the plasma with the divertor target plate with an ion flux density up to 10^{24} $m^{-2}s$ at the strike zones. The hydrogenic and impurity behaviour are routinely monitored in JET with various spectroscopic diagnostics. In particular, a visible spectrometer (KS3) and three flux cameras (KL2) are employed to routinely monitor a large number of low charge state ions, indicating hydrogenic and impurity influxes. The KS3 spectrometer is absolutely calibrated to measure the integrated photon fluxes, such as $D\alpha$ (656.1 nm) and CIII (465 nm), from both the inner and the outer divertors. The spatial distributions of bremsstrahlung (at 523.5 nm), $D\alpha$ (656.1 nm) and CII (658 nm) across the target plates are obtained from the flux cameras with interference filters. Both the diagnostics view the divertor from the top of the vessel. Fig. 9 shows the lines of sight of the KS3 visible spectrometer and the view of the KL2 flux cameras.

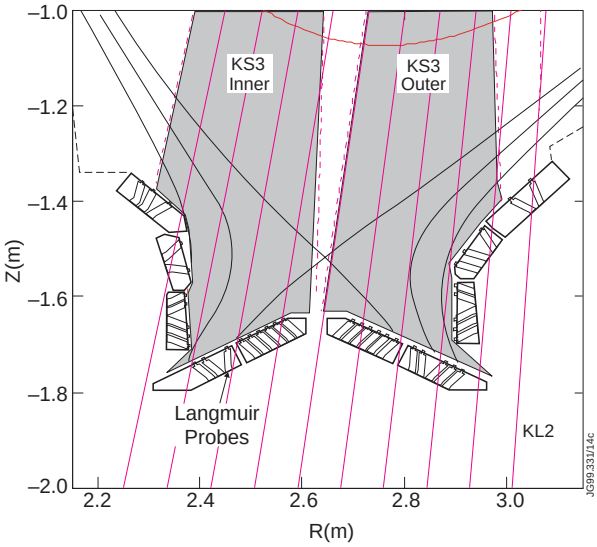

Fig.9: Vertical cross-section of the Mark II divertor showing a typical horizontal target magnetic configuration and diagnostic lines of sight of the KS3 visible spectrometer and the KL2 flux cameras. Also indicated in the figure are the fixed Langmuir probe locations.

The dominant impurity in JET is carbon [33]. One unexpected result of the Mark II divertor operation is that the carbon production yield at the divertor target is increased in the Mark II divertor relative to that in Mark I. Fig. 10 (a) shows the average *CIII* photon flux as a function of the $D\alpha$ intensity from the outer strike zones in the Mark I and Mark IIA(P) divertors for operation with the horizontal target plates. Both *CIII* and $D\alpha$ are measured simultaneously by the KS3 spectrometer. For comparison, Fig. 10 (b) shows the impurity source (CIII) versus $D\alpha$ intensity

for the discharges with the strike points placed on the vertical targets in the Mark IIA(P) and Mark IIGB divertors. Note that the comparison between the Mark I and Mark II divertors is made for the horizontal target operation since few discharges were carried out with the vertical target magnetic configuration in the Mark I divertor, whilst the vertical target configuration is selected for the Mark II /Mark IIGB comparison due to the fact that no horizontal target operation is possible in the Mark IIGB divertor due to the constraint of the septum. The data are selected from the steady-state ELMy H-mode database with NB heating power restricted between 10 and 16MW, plasma current (I_p) varying from 1 to 4.7 MA and the toroidal magnetic field (B_T) between 1 and 3.4T with a variety of magnetic configurations. The designation of the equilibria A/BBB/CC indicates target orientation: horizontal (H), vertical (V) or corner (C); flux expansion: high or standard (SFE); and triangularity: high (HT) or low (LT).

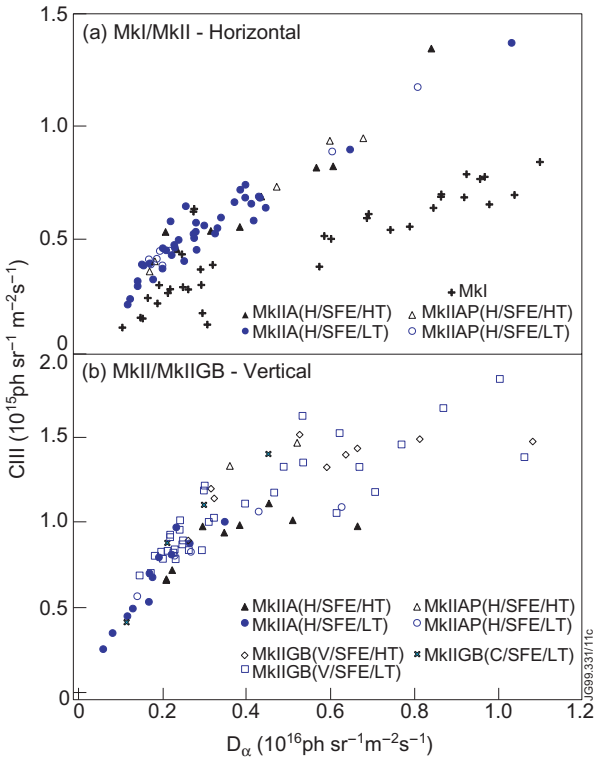

Fig.10: CIII emissions from the outer divertor as a function of the Dα photon fluxes in the Mark I, Mark IIA(P) and Mark IIGB divetors with various magnetic configurations to illustrate the changes in the impurity yield between the Mark I and Mark II divertors (a). The comparison is also made between the Mark II and Mark IIGB divertors (b).

As can be seen, the *CIII* intensity is about a factor of 2 higher in the Mark II divertor than that in the Mark I divertor for a given $D\alpha$ flux. The *CIII* and $D\alpha$ emissions from the inner divertor show similar results. It is to be noted that the electron temperature and density at the target plate are very similar for the Mark I and Mark II discharges at the strike points, as measured by the target Langmuir probes. Therefore, the higher *CIII*/$D\alpha$ ratio suggests an increased impurity production yield at the Mark II divertor target. One explanation proposed for the higher carbon yield in the Mark II divertor is that the chemical sputtering yield is increased resulting from the higher base temperature of the Mark II target plate [16] due to changes in the divertor cooling system.

In contrast, similar impurity yields have been observed in the Mark II and Mark II GB divertors, as illustrated in Fig. 10(b). In fact, both the Mark II and Mark IIGB divertor tiles are operated at a base temperature of ~500K compared with the 300K of the Mark I tiles. This further supports the hypothesis that the change in the carbon yield between the Mark I and Mark II divertors is related to the change in divertor tile temperature. Additional evidence comes from the specific experiments with reduced wall/divertor temperature performed in Mark II, which will be described in Section 3.4.

3.2 L-mode density limit

Another unexpected result in going from the Mark I divertor to the Mark II divertor is that the L-mode density limit was reduced by nearly a factor of two [20]. Fig. 11 shows the time traces of the L-mode discharges carried out in Mark I, Mark II and Mark IIGB divertors with similar NB heating to illustrate the changes in the disruptive density limit between the different divertors. The total radiated power, obtained from the bolometer measurements, is also shown. From the Mark I and Mark II data alone, it is unclear whether the lower disruptive density limit (indicated by the end of the data) in the Mark II divertor relative to the Mark I divertor is due to increased intrinsic impurity production or due to the increased closure. This is however clarified by the result from the Mark IIGB divertor. The density limit in the Mark II GB divertor was even slightly increased (about 15%) due to improved plasma purity with the improved closure, as shown in Fig. 8, compared to that in the Mark II divertor. This further supports the idea that the lower density limit in the Mark II divertor is due to increased intrinsic impurity production as opposed to the increased closure.

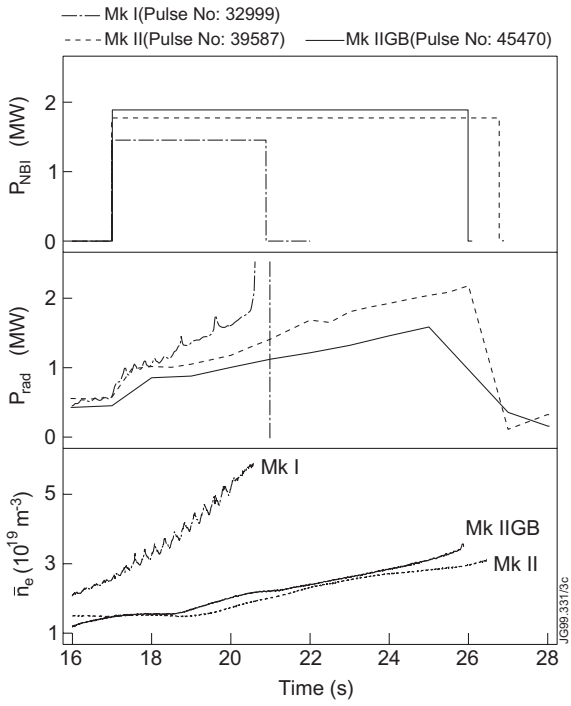

Fig.11: Comparison of the disruptive density limits in vertical target L-mode discharges between the Mark I, Mark II and Mark IIGB divertors.

It is to be mentioned that the effects of divertor geometry have been observed in the L-mode discharges for operation with the horizontal target plates. In this case, an early onset of detachment is observed at the corner of the inner divertor in contrast to the vertical target case where detachment begins at the separatrix [34,35]. This has been reproduced by B2-Eirene simulations [36] which shows that a cold and dense plasma is present at the inner divertor corner region thus promoting volume recombination. This may cause early formation of an X-point MARFE, thus reducing, at least partly, the disruptive density limit.

3.3 Edge Z_{eff} and loss power in the hot ion H-mode regime

For the low recycling hot-ion H-mode regime, the higher impurity yield at the divertor target plate manifests itself as an increase in the Z_{eff} at the edge, upstream from the target, due to poor divertor screening for the impurities for this particular regime, as will be further discussed in Section 3.5. The significance of the edge Z_{eff} for the hot-ion H-modes is that the loss power, P_{loss}, has been observed to scale as $n^2_{edge} Z_{eff,edge}$ [16, 37], as predicted by an empirical neo-classical model [38, 39]. This results in a significant increase in the loss power in the Mark II divertor

relative to that in the Mark I divertor, thus affecting the fusion performance. To illustrate this, Fig. 12 shows the edge Z_{eff} measured by the CXRS at R=3.75 ($\rho \approx 0.9$) and loss power obtained from the TRANSP analysis as a function of the line averaged density for two comparable hot-ion H-mode discharges performed in Mark I (#33643) and Mark II (#40346), respectively. The two discharges have the same horizontal target magnetic configuration at 3.8MA/3.4T with full power NB heating (~20MW). As can be seen, the Z_{eff} at the edge, at a given plasma density, is significantly higher for the discharge in the Mark II divertor. As a result, the loss power is increased in the Mark II divertor compared to the Mark I case and is consistent with the neo-classical scaling, i.e., $P_{loss} \propto n^2_{edge} Z_{eff,edge}$, as shown in the insert of Fig. 12.

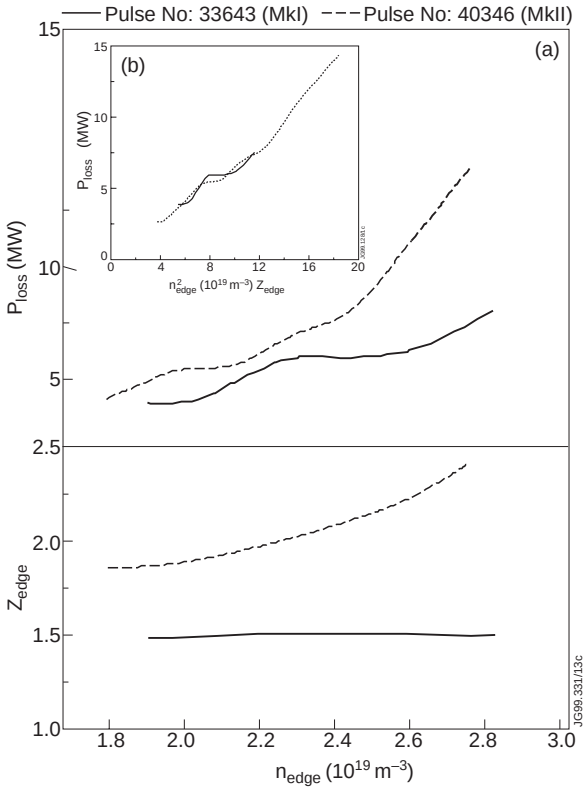

Fig.12: Comparison of Z_{eff} at the edge and loss power for hot-ion H-mode discharges in the Mark I and Mark II divertors. In the insert is shown the loss power scaling: P_{loss} vs. $n_{edge}{}^2 Z_{eff,edge}$.

3.4 Dependence on divertor target temperature

To investigate the effect of the target surface temperature on chemical sputtering, a series of dedicated experiments was carried out at the end of Mark II campaign by reducing the wall temperature from 325 to 150 °C. Consequently, the divertor tile base temperature was reduced from ~220 to ~ 120 °C through radiative cooling. Fig. 13 shows the behaviour of a pair of comparable L-mode discharges carried out before and after the temperature reduction. The two discharges have the same NB heating (2MW) and the same magnetic configuration and target orientation (vertical). The plasma line averaged density is continually increased by deuterium gas fuelling until the density limit occurs. As can be seen, for the discharge with lower wall/ target temperature both the Z_{eff} and the radiation are reduced. Detachment is also delayed compared to the discharge before temperature reduction, as indicated by the total ion fluxes to the outer target plate obtained from the fixed Langmuir probes. Consequently, the discharge with the lower wall temperature proceeds further and reaches a higher density before the disruption, with the density limit increased by ~ 20% with respect to the higher temperature case.

The detailed change in the impurity sources for the above two discharges are illustrated in Fig. 14 where the CD band emissions from the both inner and outer targets are plotted, together with the CIII emission measured along a horizontal chord through the centre of the plasma, as

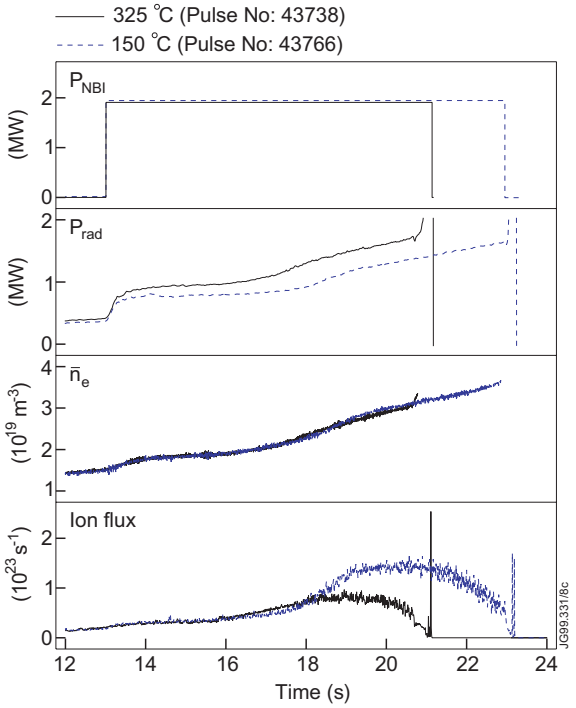

Fig.13: Global behaviour of two L-mode discharges carried out before and after the wall temperature reduction.

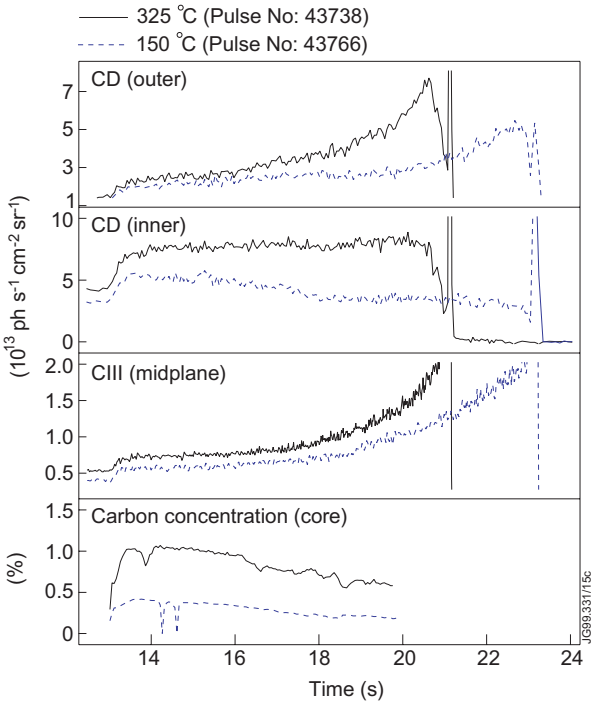

Fig.14: Comparison of the impurity sources from the divertor target and the wall in the discharges at different wall/target temperatures. The core carbon concentration is also shown.

well as the core carbon concentration, measured by the CXRS diagnostic. At reduced wall/target temperature, the impurity sources at both the inner and the outer divertor target plates are reduced, especially at the inner target, where electron temperature is lower and chemical sputtering is important. The wall source is also reduced, as indicated by the midplane CIII intensity. The core carbon concentration is hence reduced in the discharge with the lower wall temperature.

Discharges with the horizontal target magnetic equilibrium show a similar reduction in the wall and divertor carbon sources at the lower vessel wall/divertror target temperatures, resulting in an decrease in the core carbon concentration and improving the disruptive density limit, as observed in the vertical case. Fig. 15 shows the spatial distribution of D_α and CII intensities across the inner and outer target for two L-mode discharges at the horizontal target before and after the temperature reduction. Both discharges have

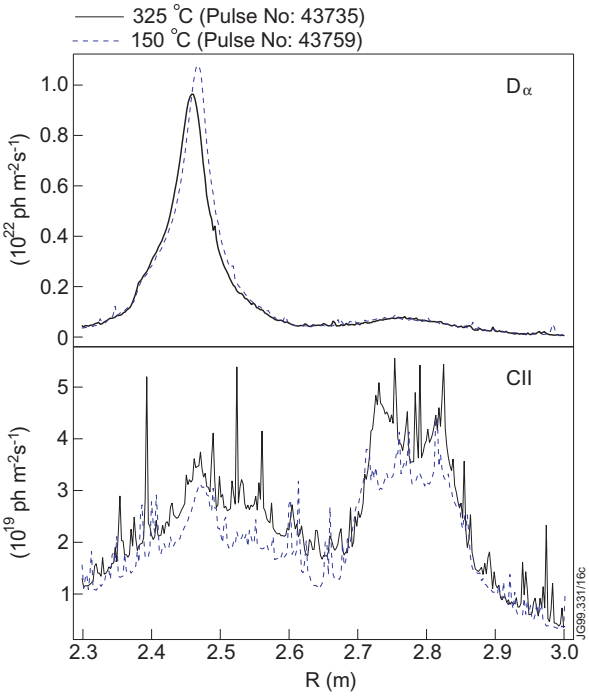

Fig.15: D_α and CII photon fluxes along the divertor target for two horizontal target L-mode discharges with the different vessel wall and divertor target temperatures.

2MW NB heating. The profiles are taken at the time when the plasma densities are the same and the particle fluxes at the target plate are also similar, as indicated by the D_α emission. It is evident that the CII photon fluxes is reduced by up to 30% for the discharge at the lower target temperature, i.e., ~120°C, compared to the discharge with the target temperature at ~220°C, as predicted by the curves of yield vs. temperature from [6].

In summary, in the discharges at the reduced vessel wall/divertor target temperatures, the carbon sources from both the wall and the target plate were reduced, hence resulting in a reduction in the core carbon concentration. In addition, the L-mode density limit was increased (by ~20%). Unfortunately, it was only possible to carry out one hot-ion discharge at the reduced wall temperature due to a subsequent water leak of the cooling system. This discharge produced a higher neutron yield than the reference discharge carried out before the wall temperature was reduced, but further experiments are required to confirm this observation. All of the effects seen here are consistent with the experimental results from the Mark I and Mark II/GB, as discussed in the previous sections (Sections 3.1 – 3.3). In contrast to expectations (based on early JET operation at 100°C), there was no difficulty in recovering from disruptions at the 150°C wall temperature.

3.5 Modelling

3.5.1 Divertor screening

In contrast to physical sputtering, chemically produced impurities have lower energy, of order of ~0.5 eV, as expected from simple molecular breakup of methane [40]. These low energy neutrals are ionised close to the divertor target where the plasma flow is strong, thus leading to prompt local redeposition [41]. In addition, hydrocarbon neutral fragments produced during the breakup processes could also be deposited across the magnetic field onto the target plates near their point of origin.

In an attempt to better understand the effect of divertor screening for the impurities and to assess the different contributions of the physical and chemical sources to the core contamination, we have carried out detailed modelling using the EDGE2D/NIMBUS [32] and DIVIMP [42,43] codes for the plasmas in different recycling regimes. DIVIMP is a Monte-Carlo impurity transport code, coupled to the 2D NIMBUS Monte-Carlo neutral code. A 2D background plasma for DIVIMP is either generated using "onion-skin" models, based on the measurements of Langmuir probes at the target plates to define boundary conditions, or taken from the EDGE2D solutions. In particular, we have selected the following cases for detailed modelling:

- Low recycling, hot-ion H-mode: Pulse 40346, horizontal target, I_p=3.8MA, B_T=3.4T.
- High recycling, ELMy H-mode: Pulse 40000, horizontal target, I_p=2.5MA, B_T=2.5T

Carbon sources at the wall and the divertor target plates are computed assuming both physical and chemical sputtering. The physically sputtered impurities are assumed to have a Thompson velocity distribution, whilst the chemically sputtered atoms are given an energy of

0.5 eV. The current available chemical sputtering data exhibit large uncertainties [6-12] and the atomic data for various hydrocarbon decomposition processes are poorly known. The actual break-up of CD_4 and other hydrocarbon products are not yet modelled by the EDGE2D/NIMBUS. In this simulation, we have used the data from Toronto [6], which was measured at low incident ion beam fluxes (10^{18} $D^+m^{-2}s^{-1}$). A yield reduction factor, α_{chem}, is used to allow for any flux dependence or prompt redeposition.

The modelling has concentrated on the ELM-free phase of the discharges with the input parameters to the EDGE2D code listed in Table 1. The cross-field transport coefficients are similar to those used in the previous simulations for the ELM-free hot-ion H-modes[16,44]. In the case of the high recycling ELMy H-mode, the inward pinch velocity is slightly reduced to match the ion saturation current (J_{sat}) and electron temperature (T_e) profiles measured by the Langmuir probes at the divertor target plates. In addition, the parallel transport is modelled with a 21 moment approach for all species [45].

Table 1 Input parameters used in the EDGE2D simulation for #40346 (low recycling) and #40000 (high recycling).

Cases	**P_{SOL} (MW)**	**n_s (10^{19} m^{-3})**	**$D_\perp$ (m^2/s)**	**$\chi^i_\perp$ (m^2/s)**	**$\chi^e_\perp$ (m^2/s)**	**V_{pinch} (m/s)**	**α_{chem}**
#40346	5.5	0.5	0.1	0.4	0.2	6	0.5
#40000	4	1	0.1	0.4	0.2	4.5	0.3

The power flux through the separatrix, P_{SOL}, is determined from the total absorbed power from the neutral beam heating, subtracting dW/dt and the radiation inside the core, taking into account the beam shine through loss, CX losses and loss to rotation, as well as the power stored in the fast ion channel, as obtained from the TRANSP analysis. In the simulation, P_{SOL} is then split into the ion channel (P_i) and the electron channel (P_e) in such way that the target parameters could be best matched. For the modelling of the low recycling hot-ion regime, little power is needed to be put into the electron channel, i.e., P_i=5.0MW, P_e=0.1MW, to reproduce the electron temperature at the target, in contrast to the high recycling case where P_i=3.0MW, P_e=1.0MW had to be assumed.

Fig. 16 compares the experimental J_{sat} and T_e profiles at the outer target plate and the modelled results for the two cases. Comparisons for the inner target plate are not considered as the experimental j_{sat} and T_e profiles are not well-defined. As can be seen, the ion flux to the target for the high recycling case (#40000) is significantly higher than that in the low recycling hot-ion case (#40346), but the electron temperature is about a factor of two lower. Fig. 17 shows the poloidal distribution of the CII photon fluxes along the divertor target for the two discharges, together with the modelled results. To reproduce the measured carbon target profiles, we have to use slightly different yield reduction factors for the two cases: α_{chem}=0.5 for the low recycling

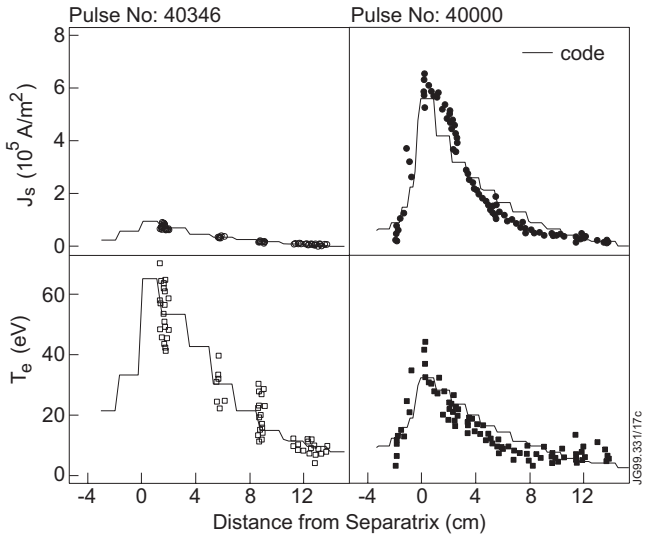

Fig.16: Comparison of experimental J_{sat} and T_e profiles along the outer target plate and the code predictions for the low recycling hot-ion H-mode (#40346) and the high recycling ELMy H-mode (#40000) discharges.

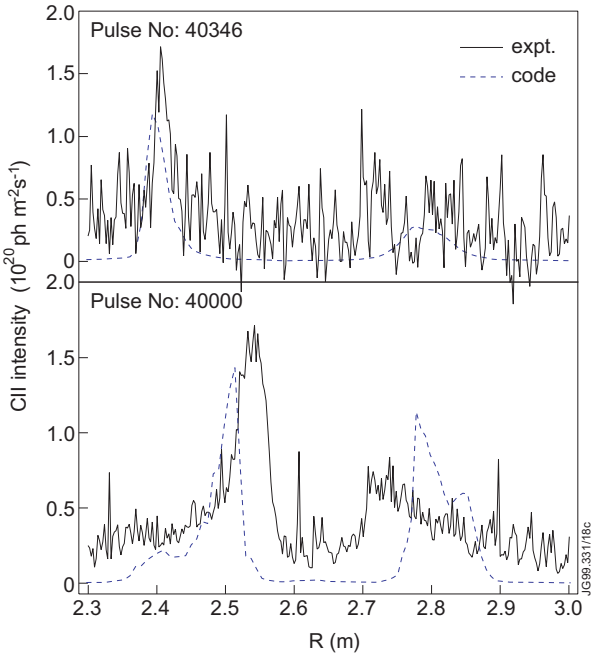

Fig.17: CII photon fluxes along the divertor target, together with the calculated results, for pulses 40346 and 40000.

(hence low ion flux) case and α_{chem}=0.3 for the high recycling case. This may be suggestive of a flux dependence of the chemical sputtering yield as: $Y_{chem} \propto \Gamma^{0.2}$, taking into account the energy dependence of the yield.

To obtain detailed impurity source distributions and the relative contribution of physical and chemical sputtering to the core contamination, we have employed the DIVIMP Monte-Carlo code as a post processor of the EDGE2D code. In this case, the 2D solutions of the EDGE2D code is directly coupled to DIVIMP as background plasma. The impurity neutrals are launched using both physical and chemical sputtering resulting from the impact of ions and atoms using the same sputtering data as in the EDGE2D simulation. The particles are then followed through each ionisation state until they redeposit on the target plates or on the wall. Fig. 18 shows the source

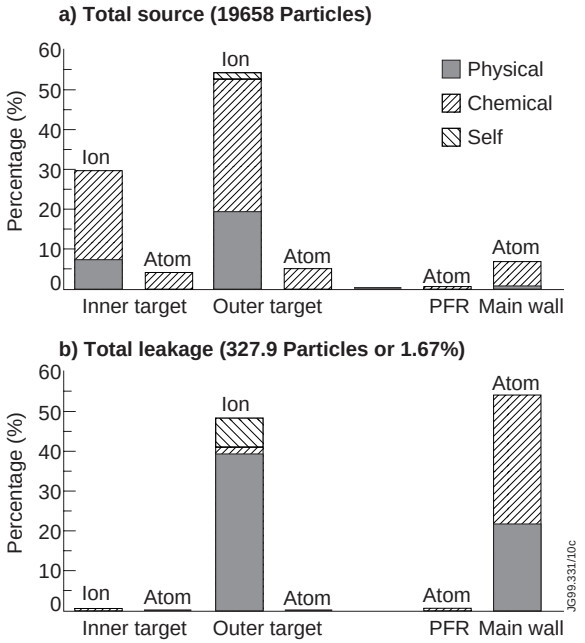

Fig.18: Source and leakage summary calculated by the EDGE2D/DIVIMP codes for the high recycling case (#40000): (a) Carbon source distribution due to physical and chemical via ion/atom impact at the inner and outer target, the private flux region (PFR) and the main chamber wall; (b) Leakage (or penetration efficiency) versus location.

distribution of carbon produced by the different sputtering processes, i.e., physical, chemical and self sputtering, together with the leakage (the amount of carbon that reaches the confined plasma) for different locations for the higher recycling case (#40000). As can be seen, the target sources dominate and the total carbon source is largest at the outer target. It appears, however, that the impurities produced at the target plates are well screened, while the wall source makes a significant contribution to core contamination. This is consistent with the experimental results from the methane puffing experiment carried out in Mark II [46]. It was observed that CD_4 puffing from the main chamber with 3×10^{21} molecules/s increased core carbon density by 40% while the same source injected in the divertor only increased core carbon by about 15%. JET previous results also showed a strong contribution from the wall source [15].

In addition, we see that chemical sputtering makes a significant contribution to the total impurity source. However the chemically produced carbon is much better screened compared to the physically sputtered source, as expected. In particular, note that the chemically sputtered impurities at the target plates are almost completely screened and make little contribution to the core carbon.

For comparison, Fig. 19 shows the EDGE2D/DIVIMP results for the low recycling case (#40346). As can be seen, the total carbon source is largest at the outer and inner divertor. However, in comparison to the high recycling case, the screening for the impurities produced in the divertor is not as good. The code predicts that the divertor source contributes significantly to the core carbon content.

In short, the results from the EDGE2D and DIVIMP modelling show the screening for the divertor impurities is strongly dependent on the plasma conditions. In particular, the codes predict that changes in divertor carbon source affect significantly the plasma purity for the low recycling regime but not for the high recycling regime.

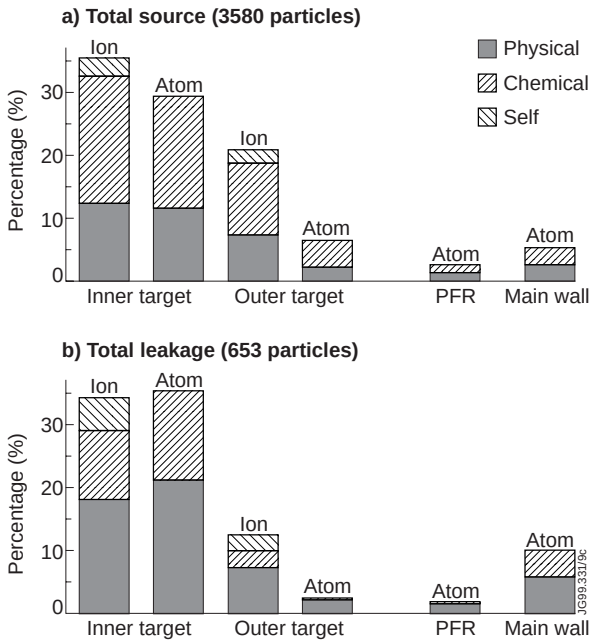

Fig.19: EDGE2D/DIVIMP calculation for the low recycling case (#40346) showing source distribution (a) and leakage (b) versus location.

3.5.2 Predictions for Mark I and Mark II

To assess quantitatively the changes in chemical sputtering yields in the Mark I and Mark II divertors and the consequence of this for the plasma purity for the low recycling hot-ion regime, we selected two of the best hot ion H-modes in Mark I and Mark II, #33643 (Mark I) and #40346 (Mark II). Similar simulations were performed for the Mark I discharge, as for the Mark II hot-ion discharge, with the same cross-transport coefficients (Table 1), but with different target plate

temperatures. In the simulation of the Mark II discharge presented in the previous section, the average surface temperature for the plasma wetted area was taken to be 400°C, which is consistent with the infra red temperature measurements, with a temperature of 300°C for other areas of the machine, whilst in the case of Mark I, the temperature rise of the wetted area of the divertor target was taken to be 100°C, but with a tile base temperature of 30°C only. For the Mark I discharge, the power flux through the separatrix (P_{SOL}) is about 5 MW, as determined from the TRANSP analysis, which is mainly put in the ion channel with only 0.1 MW in the electron channel as for the Mark II case. In addition, a separatrix density of 5.0×10^{18} m^{-3} is specified as input to the code to match the plasma parameters at the divertor target plate.

Table 2. Comparison of experimental D_α, CIII *emissions, as well as* $Z_{eff,edge}$, *together with the code predictions between #33643 (Mark I) and #40346 (Mark II).*

	33643 (MkI)			**40346 (MkII)**		
	D_α	CIII (10^{14} p/srm^{2}s)	Z_{edge}	D_α	CIII (10^{14} p/srm^{2}s)	Z_{edge}
expt.	3.0	0.7	1.49	4.2	2.1	1.9
Toronto' 97	2.8	0.8	1.46	4.1	2.0	1.8
Roth' 98	2.6	0.5	1.28	4.0	1.4	1.6

Table 2 compares the measured *CIII* and $D\alpha$ emissions from the outer divertor, with the EDGE2D results for #33643 and #40346. Both *CIII* and $D\alpha$ emissions are reproduced by the code using the Toronto chemical sputtering yield with a yield reduction factor of 0.5. In particular, the measured photon ratio *CIII/*$D\alpha$ is about a factor of two higher in #40346 (Mark II) relative to #33643 (Mark I), and is reproduced by the code taking into account the change in the temperatures between the Mark I and Mark II divertor targets. A similar calculation using the newly revised chemical sputtering formula of Roth et al. [9], also predicts the change in the chemical sputtering yield between Mark I and Mark II, as shown in Table 2.

Fig. 20 shows the EDGE2D predictions of $Z_{eff,edge}$ as a function of the separatrix density (n_s) for Mark I and Mark II with P_{SOL}=5.5MW. The simulations, which are calibrated against the hot-ion H-mode discharges described above, show that at low density the plasma is

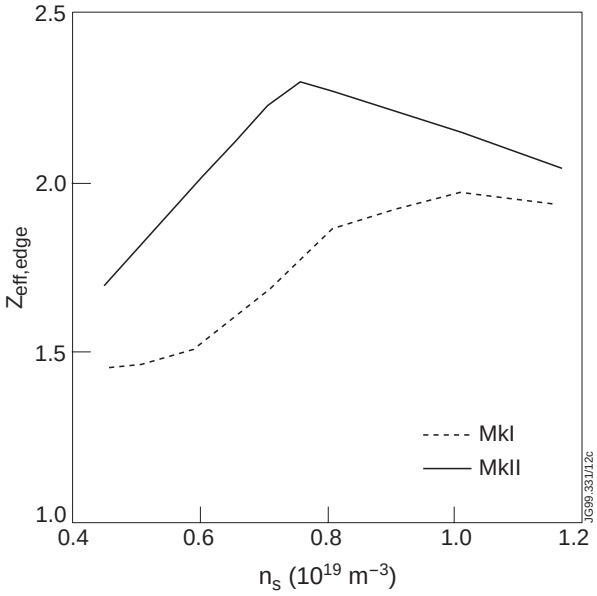

Fig.20: $Z_{eff,edge}$ *as a function of outer midplane separatrix density in Mark I and Mark II, predicted by EDGE2D simulation in which only divertor geometry is varied, with* P_{SOL}*=5.5MW.*

in the low recycling regime where the screening is poor and Z_{eff} at the edge increases with the separatrix density. In this particular regime, the edge Z_{eff}, at a given separatrix density, is significantly higher in Mark II due to increased divertor chemical sources. As n_s increases sufficiently the plasma enters the high recycling regime where screening for impurities is strong and $Z_{eff,edge}$ shows little change between Mark I and Mark II, in agreement with the experimental observations.

4. SUMMARY AND CONCLUSIONS

Increasing the divertor closure in JET has led to a significant increase in the neutral pressure in the subdivertor, hence improving deuterium pumping. The exhaust for recycling impurities has also been improved with increased divertor closure, from Mark I → Mark II → Mark IIGB, and shows a strong correlation with the subdivertor pressure or particle throughput. Experiments using simultaneous deuterium gas injection into the upstream SOL and divertor pumping show a small effect of induced SOL flow on the impurity exhaust, in contrast to the results from the "puff and pump" experiment on DIII-D [24-26], and this may be due to the large intrinsic SOL flows that are present in JET.

Helium enrichment studies have been performed under both L- and ELMy H-mode conditions in the Mark II and Mark IIGB divertors. In going from MkII to MkII GB, the helium compression is increased in step with D_2 compression. As a result, the enrichment shows little change between the two divertors. Helium enrichment decreases with plasma density or subdivertor pressure in the L-mode discharges, but remains similar in the ELMy H-mode discharges. Helium shows a significant de-enrichment with $\eta_{He}<1$. Nevertheless, in all the cases studied, helium enrichment is above the minimum requirement for ITER ($\eta_{He}\geq 0.2$). Neon, as well as argon, has enrichment factors similar to helium at low subdivertor pressure. However, neon enrichment is significantly improved at elevated pressures both in L-modes and ELMy H-modes. In particular, in the L-mode discharges, neon enrichment increases with subdivertor pressure, contrary to the helium case. This effect is related to the respective ionisation mean-free paths, and is reproduced by the EDGE2D/NIMBUS codes.

With respect to the intrinsic impurity behaviour, the divertor closure manifests itself as a decrease in Z_{eff} in L-mode discharges, as observed in the MarII and Mark IIGB divertors. The improved plasma purity leads to an improvement in the density limit (by ~15%) in the Mark IIGB divertor. In contrast, no obvious changes in Z_{eff} have been observed in the ELMy H-mode discharges [20,33], presumably due to stronger impurity sputtering at the entrance baffles of the more closed divertor geometry, thus offsetting the effect of the divertor closure.

The divertor carbon source was significantly increased in the Mark II and Mark IIGB divertors, compared to their Mark I predecessor. This dramatically reduced the disruptive density limit in the L-mode discharges in the Mark II and Mark IIGB divertors, by nearly a factor of two compared with that in the Mark I divertor. The elevated divertor source led to an increase in the

Z_{eff} at the edge, upstream from the target, in the hot-ion H-mode discharges, in contrast to the results from ELMy H-modes. For the low recycling hot-ion regime, the loss power from the confined core plasma increases with the Z_{eff} in the edge, thus reducing the fusion performance in Mark II compared to Mark I.

The increased carbon source in the Mark II and Mark IIGB divertors is attributed to the enhanced chemical sputtering at the target plate of the Mark II and Mark IIGB divertors, which have a higher base temperature (~220°C) than Mark I (~30°C). This is fully supported by the results from the specific wall/divertor temperature reduction experiment. As the wall temperature was reduced from 325°C to 150°C, and correspondingly the target temperature was reduced from ~220°C to 120°C, the impurity sources from both the wall and the divertor target were reduced by ~30% in the L-mode discharges, which is consistent with the change in chemical sputtering yield predicted by the data from Toronto [6]. Consequently, the L-mode density limit was increased by ~20%. These studies strongly suggest that for a carbon based divertor machine the operating temperature must be carefully selected in order to minimise chemical sputtering.

The screening of the impurities produced by the different sputtering processes have been studied using the EDGE2D/NIMBUS/DIVIMP codes, and shows strong dependence on the plasma conditions. In high recycling ELMy H-modes, divertor shielding for impurities is strong and the carbon source produced by chemical sputtering at the divertor target makes little contribution to the core contamination due to the lower energy carbon atoms produced compared with physical sputtering. In contrast, in the low recycling hot ion regime, the divertor screening for the impurities is poor and chemically produced divertor carbon sources contribute significantly to the core contamination. The changes in the Zeff at the edge for the hot ion H-mode discharges between Mark I and Mark II have been quantitatively reproduced by the codes taking into account the changes in chemical sputtering yields due to the different target temperatures. In addition, the codes reproduced the changes in Z_{eff} for the different regimes between Mark I and Mark II, in agreement with the experimental observations.

ACKNOWLEDEMENTS

It is a pleasure to acknowledge the contributions from the rest of the JET staff. In particular, the authors gratefully acknowledge discussions and support from P.J. Lomas, V.V. Parail and P.R. Thomas.

REFERENCES

[1] D. Reiter, G.H. Wolf, H. Kever, Nucl. Fusion **30** (1990) 2141.

[2] G. Janeschitz, for ITER-JCT and Home Teams, Plasma Phys. Control. Fusion **37** (1995) A19.

[3] W. Eckstein, J. Bohdansky, J. Roth, Atomic and Plasma-Material Interaction Data for Fusion (Supplement to Nucl. Fusion), Vol. 1, IAEA, Vienna (1991) 51.

[4] J. Roth, E. Vietzke, A.A. Haasz, ibid., p. 63.

[5] G. Federici et al., J. Nucl. Mater. **266-269** (1999) 14.
[6] B.V. Mech, A.A. Haasz, J.W. Davies, J. Nucl. Mater. **255** (1998) 153.
[7] E. Vietzke and A.A. Haasz, in : "Physical Processes of the Interaction of Fusion Plasmas with Solids", eds.: W.O. Hofer, J. Roth (Academic Press, San Diego, 1996) ch. 4, p. 135.
[8] A. Pospieszczyk, V. Philipps, E. Casarotto, et al., J. Nucl. Mater. **241-243** 91997) 833.
[9] J. Roth, C. Garc_a-Rosales, Nucl. Fusion **36** (1996) 1647 with Corrigendum, Nucl. Fusion **37** (1997) 897.
[10] A. Kallenbach et al., Nucl. Fusion **38** (1998) 1097.
[11] J. Roth, J. Nucl. Mater. **266-269** (1999) 51.
[12] R. D. Monk, C.H. Amiss, H.Y. Guo et al., "The Behaviour of the Chemical Sputtering Yield in the JET Mark I and Mark II Divertors" 8th Int. Workshop on Carbon Materials, (Jülich 1998), to appear in Physica Scripta.
[13] J. Neuhauser et al., Nucl. Fusion **24** (1984) 39.
[14] G.C. Vlases and R. Simonini, in Controlled Fusion and Plasma Physics (Proc. 18th Euro. Conf. Berlin, 1991), Vol. 15C, Part III, European Physical Society, Geneva (1991) 221.
[15] G.F. Matthews et al., J. Nucl. Mater. **196-198** (1992) 374.
[16] H.Y. Guo et al., J. Nucl. Mater. **266-269** (1999) 825.
[17] JET Team (presented by G.C. Vlases), in Fusion Energy 1996 (Proc. 16th Int. Conf. Montreal, 1996), Vol. 1, IAEA, Vienna (1997) 371.
[18] G.C. Vlases, L.D. Horton et al., J. Nucl. Mater. **266-269** (1999) 160.
[19] L.D. Horton, G.C. Vlases et al., Nucl. Fusion **39** (1999) 1.
[20] JET Team (presented by R.D. Monk), "Recent Results from Divertor and SOL Studies at JET", IAEA-CN-69/EX6/4, in Proc. 17th IAEA Fusion Energy Conference, Yokohama, Japan, 19-24 October 1998.
[21] C.F. Maggi et al., in Controlled Fusion and Plasma Physics (to appear in Proc. 26th Euro. Conf. Maastricht, 1999), European Physical Society, Geneva (1999), P1.023.
[22] A.S. Kukushkin et al., in Controlled Fusion and Plasma Physics (to appear in Proc. 26th Euro. Conf. Maastricht, 1999), European Physical Society, Geneva (1999), P4.046.
[23] S.K. Erents et al., in Controlled Fusion and Plasma Physics (to appear in Proc. 26th Euro. Conf. Maastricht, 1999), European Physical Society, Geneva (1999), P1.040.
[24] M.J. Schaffer, et al., Nucl. Fusion 35 (1995) 1000.
[25] M.J. Schaffer et al., J. Nucl. Mater. 241-243 (1997) 585.
[26] M.R. Wade et al., Nucl. Fusion 38 (1998) 1839.
[27] H.-S. Bosch et al., Phys. Rev. Lett. 76 (1996) 2499.
[28] H.-S. Bosch et al., J. Nucl. Mater. 266-269 (1999) 462.
[29] M. Groth et al., in Controlled Fusion and Plasma Physics (to appear in Proc. 25th Euro. Conf. Prague, 1998), Vol. 22C (CD-ROM), European Physical Society, Geneva (1998) 361.

[30] M. G. von Hellermann et al. in Diagnostics for Experimental Thermonuclear Fusion Reactors, edited by P E Stott, G Gorini and E Sindoni, Plenum Press, New York and London, 1996, p. 281.
[31] H.-S. Bosch et al., J. Nucl. Mater. 241-243 (1997) 82.
[32] R. Simonini et al., Contrib. Plasma Phys. 34 (1994) 368.
[33] G.M. McCracken, R. Barnsley, H.Y. Guo et al., Nucl. Fusion 39 (1999) 41.
[34] A. Loarte et al., Nucl. Fusion 38 (1998) 331.
[35] R.D. Monk et al., in Controlled Fusion and Plasma Physics (Proc. 24th Eur. Conf. Berchtesgaden 1997), Vol. 21A, Part I, European Physical Society, Geneva (1997) 117.
[36] K. Borrass et al., in Controlled Fusion and Plasma Physics (Proc. 24th Eur. Conf. Berchtesgaden 1997), Vol. 21A, Part IV, European Physical Society, Geneva (1997) 1461.
[37] H.Y. Guo et al., "Edge transport barrier in JET hot-ion H-modes", Nucl. Fusion (submitted).
[38] V.V. Parail et al, in Plasma Physics and Controlled Nuclear Fusion Research 1994 (Proc. 15th Int. Conf. Seville, 1994), Vol. 1, IAEA, Vienna (1995) 255.
[39] A. Cherubini et al., Plasma Phys. and Contr. Fusion 38 (1996) 1421.
[40] W.D. Langer et al., J. Nucl. Mater. 162-164 (1989) 329.
[41] H.Y. Guo et al., J. Nucl. Mater. 241-243 (1997) 385.
[42] P.C. Stangeby et al., Nucl. Fusion 28 (1988) 1945.
[43] P.C. Stangeby and J.D. Elder, J. Nucl. Mater. 196-198 (1992) 258.
[44] G.K. McCormick et al., J. Nucl. Mater. 241-243 (1997) 444.
[45] G. Radford, Contrib. Plasma. Phys. 32 (1992) 297.
[46] M.F. Stamp, J.D. Elder, H.Y. Guo et al., J. Nucl. Mater. 266-269 (1999) 685.